arXiv:physics/0610079v1 [physics.chem-ph] 11 Oct 2006

Ab initio potential energy surfaces, bound states and electronic spectrum of the Ar–SH complex

Richard J. Doyle
Department of Chemistry, University of Sheffield, Sheffield S3 7HF, United Kingdom

David M. Hirst
Department of Chemistry, University of Warwick, Coventry CV4 7AL, United Kingdom

Jeremy M. Hutson
Department of Chemistry, University of Durham, South Road, Durham DH1 3LE, United Kingdom

(Dated: March 31, 2022)

New *ab initio* potential energy surfaces for the $^2\Pi$ ground electronic state of the Ar–SH complex are presented, calculated at the RCCSD(T)/aug-cc-pV5Z level. Weakly bound rotation-vibration levels are calculated using coupled-channel methods that properly account for the coupling between the two electronic states. The resulting wavefunctions are analysed and a new adiabatic approximation including spin-orbit coupling is proposed. The ground-state wavefunctions are combined with those obtained for the excited $^2\Sigma^+$ state [Phys. Chem. Chem. Phys. 6, 5463 (2004)] to produce transition dipole moments. Modelling the transition intensities as a combination of these dipole moments and calculated lifetime values [J. Chem. Phys. 109, 170 (1998)] leads to a good representation of the experimental fluorescence excitation spectrum [J. Chem. Phys. 98, 4301 (1993)].

I. INTRODUCTION

Van der Waals complexes containing open-shell species are of great current interest. In particular, complexes containing atoms or molecules with orbital angular momentum necessarily involve multiple electronic states.[1,2] They provide a test-bed for studying electronically non-adiabatic effects, which are important in the theory of reaction dynamics.[3,4,5] In addition, the observation of pre-reactive Van der Waals complexes trapped in bound levels[6,7,8,9,10] can shed light on intermolecular forces in the entrance and exit channels of chemical reactions.[11,12,13,14] The form of these shallow, long-range wells can be important in determining reaction outcomes[15,16] and transition-state geometries.[17,18]

In this paper, we consider the complex consisting of an open-shell SH radical and an Ar atom. New *ab initio* potential energy surfaces (PESs) for the X $^2\Pi$ state are presented, and used in calculations of the bound rotation-vibration levels. We discuss the possibility of employing an approximate approach in the bound-state calculations, using a single adiabatic PES rather than the two surfaces used in the standard method.[1] Finally, the bound-state energies and wavefunctions are used to simulate the vibrationally resolved electronic spectrum.

The Ar–SH cluster was first detected experimentally by Miller and co-workers[19] using laser-induced fluorescence excitation spectroscopy. Subsequently this group developed empirical potential energy surfaces for the complex, for both the A state[20] and the X state,[21] by fitting model functions to reproduce laser-induced fluorescence (LIF) results. The region of the A state PES corresponding to the Ar–S-H configuration (Jacobi angles between ~ 90 and 180 degrees) was determined only approximately, because the fluorescence experiments did not probe this zone. More recently, Hirst *et al.*[22] have presented a PES for the A state based on *ab-initio* calculations at the RCCSD(T) level with the aug-cc-pV5Z basis set. This surface was used to predict bound vibrational levels in the Ar–S-H configuration[22] which have not, to our knowledge, been observed in experiment so far. A possible reason why these levels have eluded detection is discussed in section IV of this paper.

Sumiyoshi *et al.*[23] have recorded high-resolution spectra for Ar–SH in the ground electronic state using Fourier-transform microwave (FTMW) spectroscopy. These authors also produced PESs for the X state based on fitting a function to reproduce their experimental results,[23] and these surfaces were later improved with the aid of some *ab initio* results.[24] Most recently, results from microwave-millimeter-wave double-resonance spectroscopy[25] were employed to determine new three-dimensional PESs for the X state.[26]

The family of weakly bound clusters containing a rare gas atom and either the OH or SH radical have been reviewed by Carter *et al.*[27] in 2000 and by Heaven[28] in 2005.

The structure of the present paper is as follows. In Section II we present new PESs for Ar–SH ($^2\Pi$) based entirely on *ab initio* calculations at the RCCSD(T) level with an aug-cc-pV5Z basis set. In Section III we describe bound rotation-vibration level calculations using these surfaces. We also investigate the wavefunctions and introduce a new adiabatic approximation for the bound states, including spin-orbit coupling. In Section IV the results are combined with those of a previous study of the A $^2\Sigma^+$ state, in order to produce a high-quality simulation of the vibrationally resolved electronic spectrum.

II. POTENTIAL ENERGY SURFACES

The geometry of the complex is specified in terms of body-fixed Jacobi coordinates r, R and θ. R is the length of the vector $\mathbf{R}$ which links the center of mass of the SH fragment to the Ar nucleus. The vector $\mathbf{r}$ links the S nucleus to the H nucleus: its modulus r is the SH bond length. The angle between $\mathbf{R}$ and $\mathbf{r}$ is θ, so that $\theta = 0$ corresponds to a linear Ar–H-S configuration. For this work the bond length r was held constant at the experimentally determined equilibrium value of 1.3409 Å,[29] which is justified because the vibrational motion of the diatom is very weakly coupled to the relatively low-frequency Van der Waals modes of interest.

Energies were calculated for a regular grid of geometry points using the MOLPRO quantum chemistry program.[30] These points are at every distance R from 3.25 Å to 5.5 Å in steps of 0.25 Å and for every angle θ from 0° to 180° in steps of 15°. This gives a total of 130 points. We used the RCCSD(T) method (restricted coupled cluster with single, double and non-iterative triple excitations)[31,32] with the aug-cc-pV5Z basis set.[33,34,35] The counterpoise procedure of Boys and Bernardi[36] was used to correct for basis set superposition error (BSSE). This is the same level of theory and basis set as were used in recent calculations of the PES for the A-state of Ar–SH.[22]

Two potential surfaces were obtained from the *ab initio* calculations. These correspond to two adiabatic electronic states: one symmetric (A') and one antisymmetric (A'') with respect to reflection in the plane of the nuclei. The two states are degenerate at linear geometries but nondegenerate at nonlinear geometries: the splitting is an example of the Renner-Teller effect. The interaction energies for each state were interpolated using a 2D spline function, and contour plots of the resulting surfaces are shown in Fig. 1. The A' and A'' surfaces result from the electronic Hamiltonian without spin-orbit coupling: a discussion of surfaces including spin-orbit coupling is presented in section IV.

The adiabatic surfaces (adiabats) are qualitatively similar to those reported for He–SH and Ne–SH complexes.[37] The latter were calculated at the RCCSD(T) level, using the smaller aug-cc-pVTZ basis set, but with an additional set of bond functions, and counterpoise correction. A comparison of the positions and energies of the minima on the Ar–SH surfaces presented here with those for X-state He–SH and Ne–SH is given in Table I. For all the A'' surfaces there is a global minimum in the linear X–S-H configuration (where X is He, Ne or Ar) and a local minimum in the linear X–H-S configuration. The X–H-S configurations are saddle points on the A' surfaces, which have shallow local minima at $\theta = 180°$ and global minima at nonlinear configurations. The A' global minima are deeper than those on the A'' surfaces, because in the A' state the SH π hole is directed towards the Ar atom, resulting in reduced repulsion. The global minima for the A' state occur at angles θ that increase with the atomic number of the rare gas atom. Also, as expected, the minima are deeper for clusters containing heavier (and more polarizable) rare gas atoms.

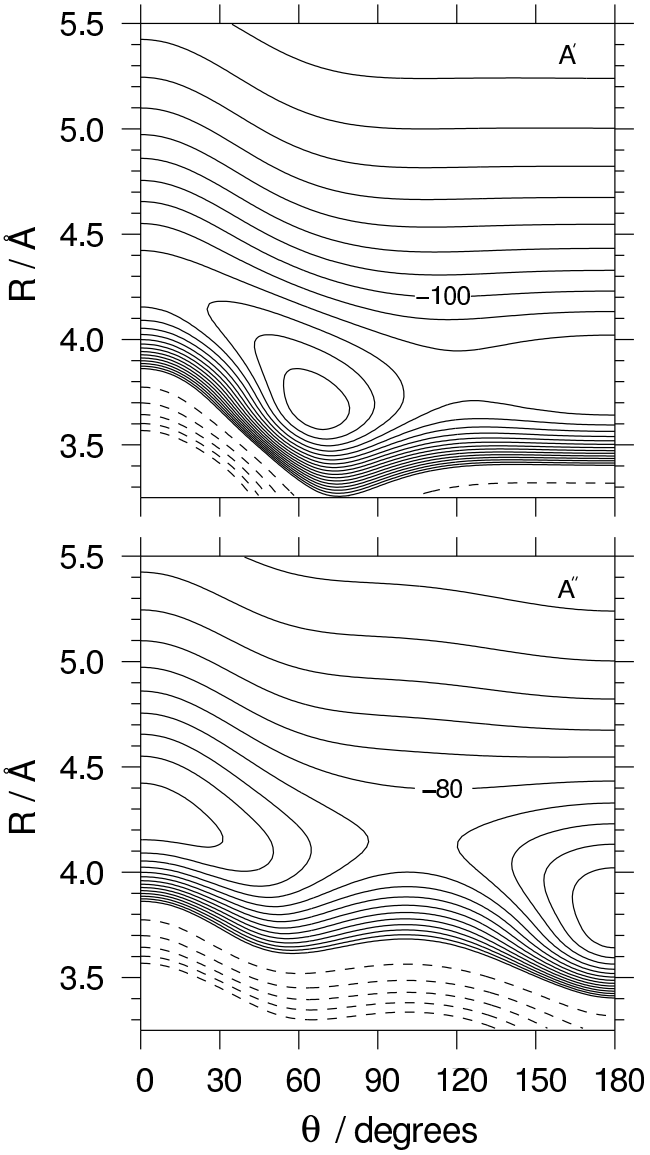


FIG. 1: *Ab initio* potential energy surface contour plots for Ar–SH (X) in the A' state (upper plot) and the A'' state (lower plot). Solid contour lines are shown at 10 cm^{-1} intervals, ranging from 0 cm^{-1} to −150 cm^{-1} inclusive for the A' surface and 0 cm^{-1} to −120 cm^{-1} inclusive for the A'' surface. Dashed contour lines are shown at 100 cm^{-1} intervals from +100 cm^{-1} to +500 cm^{-1} inclusive for both surfaces. The linear Ar–H-S conformation corresponds to $\theta = 0°$.

In order to perform dynamical calculations on Ar–SH, we need to evaluate the matrix elements of the potential between electronic states labelled with an angular momentum quantum number λ. For this purpose it is convenient to re-express the potential energy surfaces as

TABLE I: Positions and well depths of potential minima on the A' and A'' adiabatic surfaces for the X-state of SH–rare gas clusters. The results for Ne–SH and He–SH clusters are from ref. 37.

Cluster	State	R/Å	θ/°	depth/cm^{-1}
Ar–SH	A'	3.678	66.6	157.69
Ne–SH	A'	3.611	57.2	57.05
He–SH	A'	3.639	54.4	25.97
Ar–SH	A' and A''	3.801	180	128.54
Ne–SH	A' and A''	3.593	180	54.27
He–SH	A' and A''	3.593	180	25.27
Ar–SH	A''	4.274	0	125.22
Ne–SH	A''	4.101	0	45.75
He–SH	A''	4.126	0	21.16

the sum (V_0) and difference (V_2) potentials

$$V_0(R,\theta) = \frac{1}{2}\left[V_{A'}(R,\theta) + V_{A''}(R,\theta)\right],$$

$$V_2(R,\theta) = \frac{1}{2}\left[V_{A'}(R,\theta) - V_{A''}(R,\theta)\right].$$

Contour plots of these surfaces are shown in Fig. 2. They are quite similar to those recently presented by Sumiyoshi *et al.*[26] The latter were fitted to reproduce experimental results, with starting values for the potential parameters obtained from *ab initio* calculations (RCCSD(T)/aug-cc-pVTZ). The form of our sum potential is also qualitatively similar to those recently presented for Ne–SH and Kr–SH by Suma *et al.*[38]

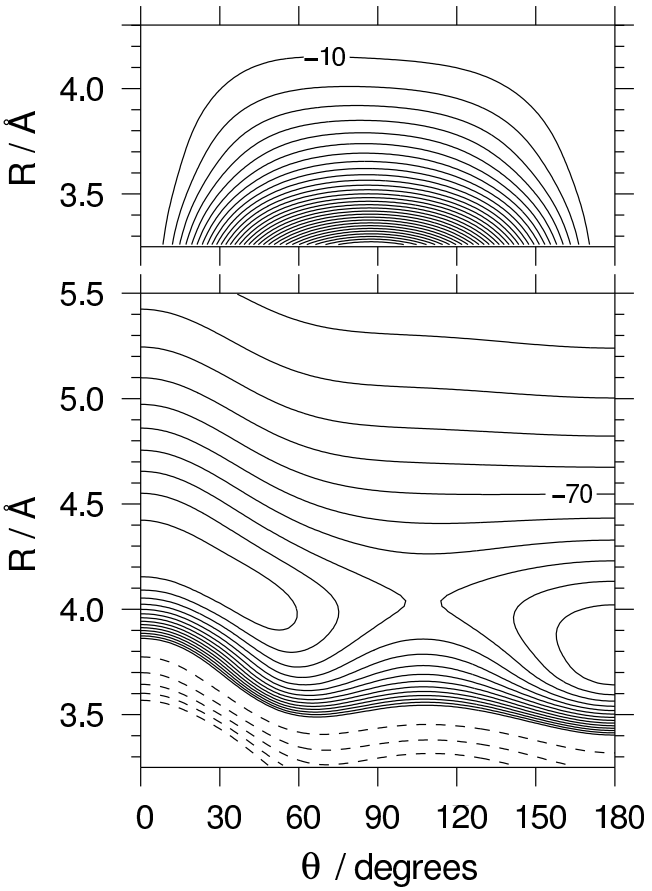


FIG. 2: Contour plots for the Ar–SH (X) difference (upper plot) and sum (lower plot) potential energy surfaces. Solid contour lines are shown at 10 cm^{-1} intervals, ranging from 0 cm^{-1} to −300 cm^{-1} inclusive for the difference surface and from 0 cm^{-1} to −120 cm^{-1} inclusive for the sum surface. Dashed contour lines are shown at 100 cm^{-1} intervals from +100 cm^{-1} to +500 cm^{-1} for the sum surface only. The linear Ar–H-S conformation corresponds to $\alpha = 0°$.

III. BOUND-STATE CALCULATIONS

A. Coupled channel calculations

The bound states of a complex such as Ar–SH ($X^2\Pi$) involve *both* potential energy surfaces. In the present work we use a coupled-channel approach to calculate the bound states. In a body-fixed axis system the Hamiltonian operator is

$$H = -\frac{\hbar^2}{2\mu}R^{-1}\left(\frac{\partial^2}{\partial R^2}\right)R + H_{\rm mon} + \frac{\hbar^2(\hat{J}-\hat{j})^2}{2\mu R^2} + \hat{V}, \quad (1)$$

where $H_{\rm mon}$ is the monomer Hamiltonian and $\hat{V}$ is the intermolecular potential. In a full treatment including overall rotation, the total wavefunction of the complex may be expanded[1]

$$\Psi_n^{JM} = R^{-1}\sum_{jP\lambda\sigma}\Phi_{jP;\lambda\sigma}^{JM}\,\chi_{Pn;j;\lambda\sigma}^{J}(R), \quad (2)$$

where the channel basis functions are

$$\Phi_{jP;\lambda\sigma}^{JM} = \varphi_\sigma\varphi_\lambda \quad \left(\frac{2j+1}{4\pi}\right)^{\frac{1}{2}} D_{P\omega}^{j*}(\phi,\theta,0)$$

$$\times \quad \left(\frac{2J+1}{4\pi}\right)^{\frac{1}{2}} D_{MP}^{J*}(\alpha,\beta,0), \quad (3)$$

The monomer basis functions are labelled by Hund's case (a) quantum numbers λ and σ, the projections of the electronic orbital and spin angular momentum along the SH axis, and $\omega = \lambda+\sigma$.[52] λ, σ and ω are all signed quantities. The D functions are Wigner rotation matrices.[39] The first D function describes the rotation of the monomer with respect to body-fixed axes, with angular momentum quantum number j (including electronic orbital and spin angular momentum) and projection P along the intermolecular vector $\mathbf{R}$. The second D function describes the rotation of the complex as a whole, with total angular momentum J and projections M and P onto space-fixed and body-fixed axes respectively. The angles (β,α) describe the orientation of the $\mathbf{R}$ vector in space.

The monomer Hamiltonian used here for SH($X^2\Pi$) is[40]

$$H_{\rm mon} = b(\hat{j}-\hat{l}-\hat{s})^2 + H_{\rm so}, \quad (4)$$

where the rotational constant b is 9.465 cm^{-1}.[29] For simplicity the spin-orbit Hamiltonian $H_{\rm so}$ is taken to be independent of R and θ and equal to $a\lambda\sigma$, with $a = -378.5$ cm^{-1}.[29]

It is convenient to expand the sum and difference potentials in terms of renormalized spherical harmonics $C_{lm}(\theta,\phi)$,

$$V_0(R,\theta) = \sum_l V_{l0}(R) C_{l0}(\theta,0); \quad (5)$$

$$V_2(R,\theta) = \sum_l V_{l2}(R) C_{l2}(\theta,0). \quad (6)$$

The potential matrix elements between the angular basis functions may then be written

$$\langle JM; jP; \lambda\sigma|\hat{V}|JM; j'P'; \lambda'\sigma'\rangle = \delta_{PP'}\delta_{\sigma\sigma'} \sum_l V_{l,|\lambda-\lambda'|}(R)\, g_{l,\lambda-\lambda'}(j\omega; j'\omega'; P), \quad (7)$$

where the potential coupling coefficients are

$$g_{l,\lambda-\lambda'}(j\omega; j'\omega'; P) = (-1)^{P-\omega}\left[(2j+1)(2j'+1)\right]^{\frac{1}{2}} \times \begin{pmatrix} j & l & j' \\ -\omega & \lambda-\lambda' & \omega' \end{pmatrix} \begin{pmatrix} j & l & j' \\ -P & 0 & P \end{pmatrix}. \quad (8)$$

The potential matrix elements are independent of J and diagonal in P. Nevertheless, in a full treatment the wavefunctions of the complex are linear combinations of functions with different values of P, because the operator $(\hat{J}-\hat{j})^2$ in Eq. 1 has matrix elements off-diagonal in P ($\Delta P = \pm 1$). However, the full wavefunctions are eigenfunctions of the parity operator: symmetrized basis functions may be constructed by taking even and odd linear combinations of $\Phi^{JM}_{jP;\lambda\sigma}$ and $\Phi^{JM}_{j-P;-\lambda-\sigma}$.

In the present work, the coupled equations are solved using the BOUND program of Hutson.[41] The wavefunction log-derivative matrix is propagated outwards from a boundary point at short range ($R_{\rm min}$) and inwards from a boundary point at long range ($R_{\rm max}$) to a matching point ($R_{\rm mid}$) in the classically allowed region. If E is an eigenvalue of the Hamiltonian, the determinant of the difference between the two log-derivative matrices at $R_{\rm mid}$ is zero.[42,43] The BOUND program locates eigenvalues by searching for zeroes of the lowest eigenvalue of the matching determinant,[43] using bisection followed by the secant method. In the present work we use $R_{\rm min} = 3.0$ Å, $R_{\rm max} = 9.5$ Å, $R_{\rm mid} = 4.2$ Å and a log-derivative sector size of 0.02 Å. The basis set includes all SH functions up to $j_{\rm max} = 15/2$ in both spin-orbit manifolds.

The energies obtained from full close-coupling calculations for the lowest few $J = 3/2$ levels of Ar–SH (actually carried out in the equivalent space-fixed basis set[1]) are shown in Table II. These levels all correlate with SH $^2\Pi_{3/2}$, $j = 3/2$ and are labelled with the projection quantum number P and Van der Waals stretching quantum number n. We use the convention that levels in which P and ω for the dominant basis functions have the *same* sign are labelled with positive P and those where they have *different* sign are labelled with negative P.[1] In order of increasing energy, the lowest four levels for Ar–SH have $P = +3/2$, $+1/2$, $-3/2$, $-1/2$, in contrast to Ar–OH where the order is $+3/2$, $+1/2$, $-1/2$, $-3/2$.[1,44] The difference is due to the anisotropy of the sum potential $V_0(R,\theta)$: the ratio V_{20}/V_{10} is larger for Ar–SH.

TABLE II: Bound-state energies for $J = 3/2$ levels of Ar–SH from full close-coupling calculations (average $E_{\rm CC}$ and parity splitting $\Delta E_{\rm CC}$), helicity decoupling calculations ($E_{\rm HD}$) and single-surface calculations on the lower adiabatic surface including spin-orbit coupling ($E_{\rm Ad}$). All energies are relative to the dissociation energy to form SH ($X^2\Pi_{3/2}$, $j = 3/2$). All energies are given as wavenumbers in cm^{-1}.

P	n	$E_{\rm CC}$	$\Delta E_{\rm CC}$	$E_{\rm HD}$	$E_{\rm Ad}$
$+3/2$	0	-102.745	$+3.5\times10^{-5}$	-102.652	-102.725
$+1/2$	0	-97.766	$+0.144$	-97.593	-97.667
$-3/2$	0	-94.940	-1.1×10^{-3}	-94.894	-95.035
$-1/2$	0	-92.116	-0.138	-92.222	-92.293
$+3/2$	1	-77.292	$+2.6\times10^{-5}$	-77.111	-77.258
$+1/2$	1	-72.276	$+0.134$	-72.100	-72.148
$-3/2$	1	-69.356	-1.3×10^{-3}	-69.265	-69.382
$-1/2$	1	-67.207	-0.124	-67.291	-67.315

The close-coupling results may be compared with the microwave experiments of Sumiyoshi *et al.* ,[23] who obtained a rotational constant $B^{\rm eff} = 1569.66$ MHz (0.05236 cm^{-1}) and parity doubling constant $q_J = 0.32873$ MHz (1.10×10^{-5} cm^{-1}) for the ground state ($P = +3/2$). These correspond to a $J = 3/2 - 5/2$ separation of 0.262 cm^{-1} and a $J = 3/2$ parity splitting of 6.6×10^{-5} cm^{-1}, which compare with calculated values of 0.263 cm^{-1} and 3.5×10^{-5} cm^{-1} respectively. The very good agreement for the rotational spacing suggests that the equilibrium distance of our *ab initio* potential is quite accurate. The difference of almost a factor of 2 in the parity splitting is less satisfactory, but Dubernet *et al.*[45] have shown that such terms involve complicated combinations of high-order terms involving the difference potential, spin uncoupling and Coriolis perturbations. Small differences between the energies of excited states can have a large effect on the parity splitting. Sumiyoshi *et al.*[25] have very recently measured microwave–millimetre-wave double-resonance spectra of the $P = +1/2 \leftarrow +3/2$ band of Ar–SH. The centre of gravity of the parity components of the $J = 3/2 \leftarrow 1/2$ line is 81.8 GHz (2.73 cm^{-1}). The corresponding calculated quantity from our potential is 4.805 cm^{-1}. In addition, the measured parity splitting for the $J = 3/2$, $P = +1/2$ level is about 5300 MHz (0.177 cm^{-1}), which compares with 0.144 cm^{-1} from our calculations. An interesting possibility for future work would be to adjust the *ab initio* potential to improve the fit to the spectroscopic parameters using the morphing

procedure of Meuwly and Hutson.[46]

B. Wavefunctions

The full wavefunctions (Eq. 2) contain contributions from all possible values of P and ω and are not separable between the body-fixed angles (θ, ϕ) and the space-fixed angles (β, α). This makes them hard to visualize. In addition, since the mixings depend on the total angular momentum J, they are not convenient for calculating band intensities. We therefore introduce two approximations to simplify the description of the wavefunctions for this purpose. First, we introduce the *helicity decoupling* approximation, where matrix elements of $(\hat{J} - \hat{j})^2$ off-diagonal in P are neglected. Secondly, we neglect matrix elements of $H_{\rm mon}$ off-diagonal in σ (spin-uncoupling terms). The coupled equations then simplify to

$$\left[-\frac{\hbar^2}{2\mu}\frac{d^2}{dR^2} + E^{\rm mon}_{\omega j} + \frac{\hbar^2}{2\mu R^2}\left(J(J+1) + j(j+1) - 2\omega^2\right) - E^J_{Pn}\right]\chi^J_{Pn;j;\lambda\sigma}(R) = -\sum_{j'\lambda'}\langle JM; j'P\lambda'\sigma|\,\hat{V}\,|JM; jP\lambda\sigma\rangle\,\chi^J_{Pn;j';\lambda'\sigma}(R). \quad (9)$$

Since all matrix elements off-diagonal in P and σ have been neglected, states with quantum numbers (P, ω) and $(-P, -\omega)$ are uncoupled and it is not necessary to take combinations of definite total parity. However, states with (P, ω) and $(-P, \omega)$ or $(P, -\omega)$ have different potential energies and are nondegenerate.

The energy levels obtained from helicity decoupling calculations for Ar–SH are included in Table II. The approximation is accurate to about 0.2 cm^{-1} for $n = 0$ and 1, but is less reliable for higher states. In particular, the region between -60 and -40 cm^{-1} contains both $j = 3/2,\ n = 2$ and $j = 5/2,\ n = 0$ levels. In the presence of the resulting near-degeneracies, the terms that are omitted in the approximate Hamiltonian can cause quite significant level shifts.

In the helicity decoupling approximation, P is a good quantum number. However, ω is not because V_2 mixes levels with $\Delta\lambda = \pm 2$ (but $\Delta\sigma = 0$) and thus mixes $\omega = +3/2$ with $-1/2$ and $\omega = +1/2$ with $-3/2$. However, in the absence of terms off-diagonal in σ the two sets are not mixed with one another. Each wavefunction thus has only *two* components corresponding to different values of ω. The wavefunctions may be written

$$\Psi^J_{Pn} = \sum_\omega \chi^J_{Pn;\omega}(R, \theta)\,\Phi^{JM}_{P;\lambda\sigma}, \quad (10)$$

where the basis functions now exclude the θ-dependence,

$$\Phi^{JM}_{P;\lambda\sigma} = \varphi_\sigma\varphi_\lambda\left(\frac{2J+1}{8\pi^2}\right)^{1/2} D^{J*}_{MP}(\alpha, \beta, \phi), \quad (11)$$

and the 2-dimensional functions that characterize the components of the wavefunction for each ω are

$$\chi^J_{Pn;\omega}(R, \theta) = \sum_j \left(j + \tfrac{1}{2}\right)^{1/2} d^j_{P\omega}(\theta)\chi^J_{Pn;j;\lambda\sigma}(R), \quad (12)$$

where $d^j_{j\omega}(\theta)$ is a reduced rotation matrix.[39]

We have adapted the BOUND program[41] to calculate wavefunctions for this case by back-substituting into the log-derivative propagation equations, as described for the closed-shell (single surface) case by Thornley and Hutson.[47] Examples of the resulting wavefunctions $\chi^J_{Pn;\omega}(R, \theta)$ are shown in Fig. 3. It may be seen that the components for different values of ω have quite different radial and angular distributions.

The Ar–SH wavefunctions are qualitatively similar to those for Ne–SH obtained by Cybulski *et al.*[37] Since the potential anisotropy for Ar–SH is only a few tens of cm^{-1} in the well region, there is only weak mixing of SH rotational functions with different values of j. For this reason the wavefunctions are dominated by the functions $d^{3/2}_{P\omega}(\theta)$, as described by Dubernet and Hutson[1] for the case of Ar–OH. The d functions are shown, for example, in Fig. 7 of ref. 1 and the angular parts of the wavefunctions of Fig. 3 follow them quite closely.

C. Adiabatic approximations

In a basis set of Hund's case (a) functions with signed values of $\lambda = \pm 1$ and $\sigma = \pm 1/2$, we can define new adiabatic surfaces (adiabats) including spin-orbit coupling as eigenvalues of the Hamiltonian matrix at each value of R and θ,

$$\begin{pmatrix} V_0 + \frac{1}{2}a & 0 & V_2 & 0 \\ 0 & V_0 - \frac{1}{2}a & 0 & V_2 \\ V_2 & 0 & V_0 - \frac{1}{2}a & 0 \\ 0 & V_2 & 0 & V_0 + \frac{1}{2}a \end{pmatrix}, \quad (13)$$

where again the spin-orbit Hamiltonian is taken to be simply $a\lambda\sigma$. This clearly factorizes into two equivalent 2×2 matrices, one containing $\omega = +3/2$ and $-1/2$ and the other containing $\omega = +1/2$ and $-3/2$. The resulting adiabats may be designated $V_+(R, \theta)$ and $V_-(R, \theta)$ with

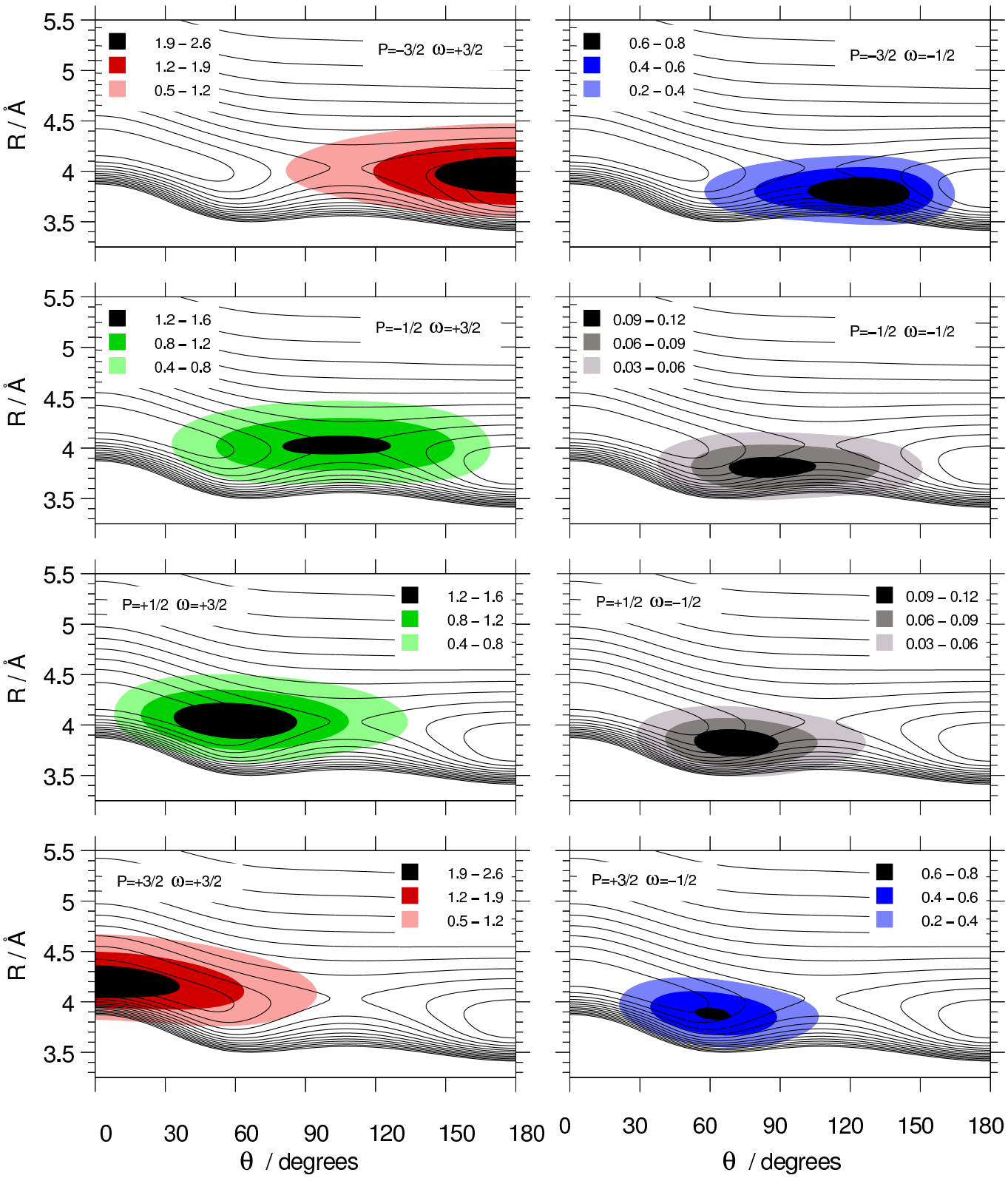


FIG. 3: [Colour Figure] Contour plots of the wavefunction components, superimposed on the average potential.

corresponding electronic functions $\psi_+(R,\theta)$ and $\psi_-(R,\theta)$ given by

$$\begin{pmatrix}\psi_+(R,\theta)\\ \psi_-(R,\theta)\end{pmatrix} = \begin{pmatrix}\cos\alpha_{\rm ad}(R,\theta) & \sin\alpha_{\rm ad}(R,\theta)\\ -\sin\alpha_{\rm ad}(R,\theta) & \cos\alpha_{\rm ad}(R,\theta)\end{pmatrix}\begin{pmatrix}\varphi_{\pm 3/2}\\ \varphi_{\mp 1/2}\end{pmatrix} \quad (14)$$

where $\varphi_\omega = \varphi_\lambda\varphi_\sigma$. The adiabats for Ar–SH are shown in Fig. 4. Since for Ar–SH $V_2(R,\theta)$ is small compared to a in the well region, the lower adiabat is always predominantly $\omega = \pm 3/2$ in character and the upper adiabat is always predominantly $\omega = \mp 1/2$ in character. The corresponding mixing angle $\alpha_{\rm ad}$ is 0 at $\theta = 0$ and 180° (where $V_2(R,\theta) = 0$) and less than 20° at other angles for $R > 3.5$ Å. A contour plot of the mixing angle is shown in Fig. 5.

A further consequence of the large spin-orbit coupling constant is that both adiabats resemble the *sum* potential $V_0(R,\theta)$ much more than the A' and A'' potentials. The spin-orbit coupling has in effect quenched the splitting between the A' and A" states. This explains why there is no tendency for the wavefunctions shown in Fig. 3 to "fall into" the non-linear minimum of the A' state.

The existence of adiabats including spin-orbit coupling suggests a Born-Oppenheimer separation in which the total wavefunctions are written approximately as

$$\Psi_{iPn} \approx R^{-1}\psi_i(R,\theta)\chi_{iPn}(R,\theta), \quad (15)$$

where ψ_i is one of the functions of Eq. 14 and $\chi_{in}(R,\theta)$ is a solution of an effective Schrödinger equation of the form

$$\left[-\frac{\hbar^2}{2\mu}\frac{\partial^2}{\partial R^2} + H_{\rm rot} + \frac{\hbar^2(\hat{J}-\hat{\jmath})^2}{2\mu R^2} + V_i(R,\theta) - E_{iPn}\right]\chi_{iPn}(R,\theta) = 0. \quad (16)$$

However, the appropriate angular operator $H_{\rm rot}$ to use in such a calculation is hard to define. The reduced rotation matrices $d^j_{P\omega}(\theta)$ that describe the free SH molecule are eigenfunctions of $H_{\rm rot} = b(\hat{\jmath}^2 - 2\omega^2)$, where

$$\hat{\jmath}^2 = \left[-\frac{1}{\sin\theta}\frac{\partial}{\partial\theta}\left(\sin\theta\frac{\partial}{\partial\theta}\right) + \frac{P^2+\omega^2-2P\omega\cos\theta}{\sin^2\theta}\right]. \quad (17)$$

This contains singularities at $\theta = 0$ and/or 180° that depend on the values of P and ω. However, there is no single value of ω that is appropriate at all configurations. The simplest approach is to replace ω in Eq. 17 with the value that is appropriate at $\theta = 0$ and 180° and solve Eq. 16 in a basis set of d functions for each value of P. This is equivalent to solving the coupled equations using a basis set containing only functions with a single value of ω. The results obtained with this approximation are included in Table II: it may be seen that it gives energies that are generally slightly too low (compared to the helicity decoupling results), by 0.05 to 0.15 cm^{-1}. A slightly better but significantly more complicated approximation would be to replace ω with $\langle\omega\rangle$ and ω^2 with $\langle\omega^2\rangle$ in Eq. 17 to give an improved effective potential.

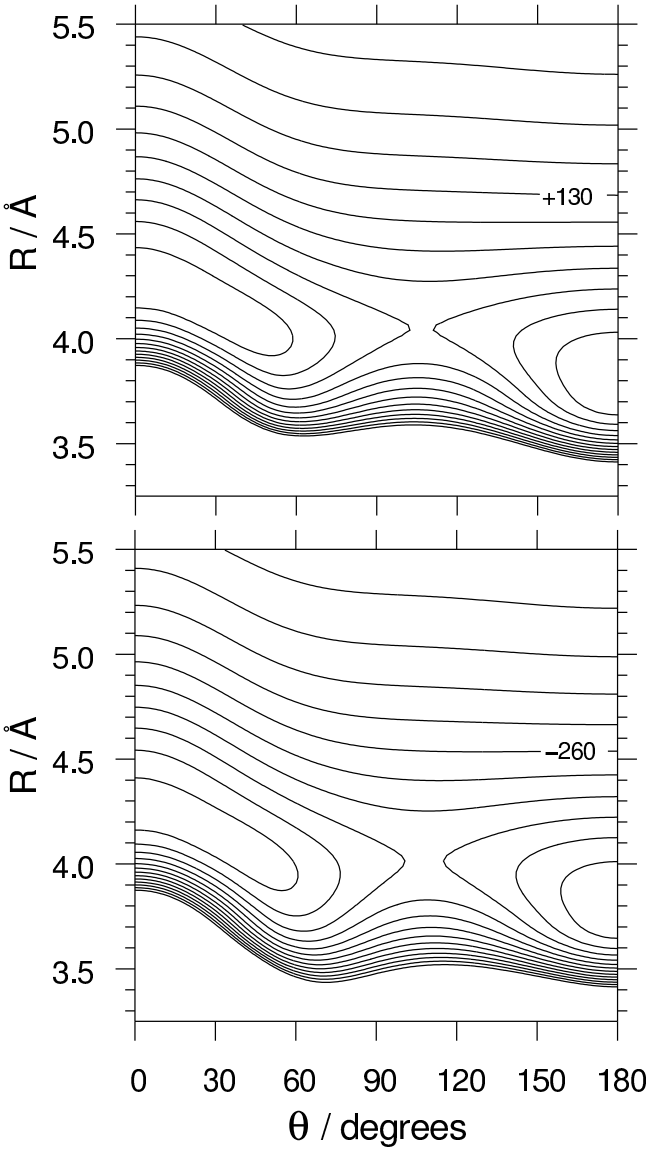


FIG. 4: Contour plots for Ar–SH (X) adiabats including spin-orbit coupling. Contour lines are shown at 10 cm^{-1} intervals, ranging from 70 cm^{-1} to $+a/2$ for the upper surface and from -310 cm^{-1} to $-a/2$ for the lower surface.

One approach that is clearly *not* appropriate is to carry out a bound-state calculation on a single adiabat $V_\pm(R,\theta)$ assuming that the SH molecule behaves as a closed-shell rigid rotor. Such a calculation would give substantially incorrect energies and wavefunctions.

It is in fact true that *no wavefunction of the form (15) can have the correct behavior near both linear geometries.* To see this, consider an alternative definition of the mixing angle that can be obtained from a single wavefunction

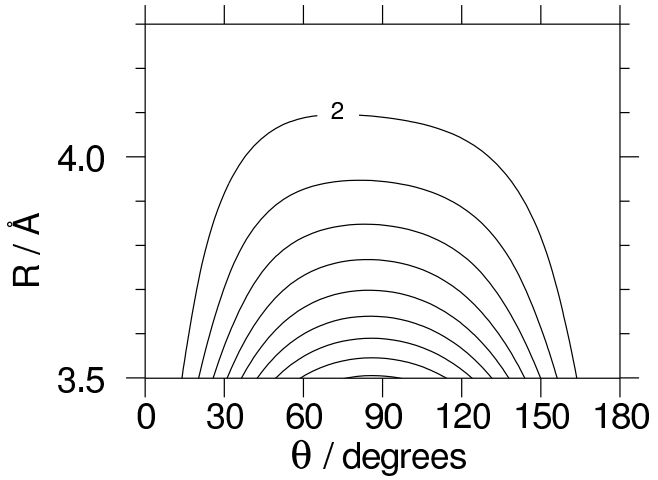


FIG. 5: Contour plot of the adiabatic mixing angle $\alpha_{\rm ad}$. This angle is derived from the adiabats and is defined in Eq. 14. The contour lines are spaced at 2° intervals.

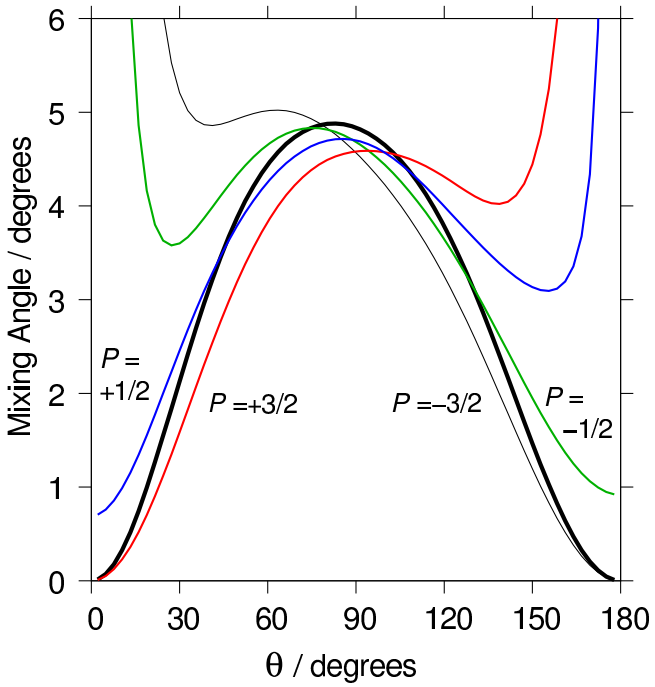


FIG. 6: [Colour Figure] Comparison of the adiabatic mixing angle $\alpha_{\rm ad}$ (thick black line) with angles obtained from wavefunctions correlating with $j = 3/2$, $\omega = +3/2$ for $P = +3/2$ (red), $P = +1/2$ (blue), $P = -1/2$ (green) and $P = -3/2$ (black). The mixing angles are shown as cuts through the corresponding surfaces taken at $R = 3.9$ Å.

in the helicity decoupling approximation,

$$\tan\alpha^J_{Pn}(R,\theta) = \frac{\chi^J_{Pn;\mp1/2}(R,\theta)}{\chi^J_{Pn;\pm3/2}(R,\theta)}. \qquad (18)$$

This quantity is plotted for $n = 0$ and all four P values corresponding to $j = 3/2$ in Fig. 6. The mixing angles for $P = +3/2$ and $P = +1/2$ bear some similarity to $\alpha_{\rm ad}(R,\theta)$ (Fig. 5) at small θ, but tend to 90° instead of zero at $\theta = 180°$. Conversely, the mixing angles for $P = -3/2$ and $P = -1/2$ tend to 90° at $\theta = 0$. This is easy to explain in terms of the reduced rotation matrices that appear in Eq. 12. For example, the functions $d^j_{\pm3/2,\pm3/2}(\theta)$ all behave as $\cos^3(\theta/2)$ as $\theta \to 180°$, while the functions $d^j_{\mp1/2,\pm3/2}(\theta)$ behave as $\cos(\theta/2)$. This corresponds to $\tan\alpha^J_{3/2,n} \to \infty$ as $\theta \to 180°$ so $\alpha^J_{3/2,n} \to 90°$ in that limit. The point here is that the component of the $P = +3/2$ wavefunction on the $\omega = -1/2$ surface goes to zero more slowly than that on the $\omega = +3/2$ surface as $\theta \to 180°$. Fig. 5 shows that the coupled-channel wavefunctions (10) for $P = +3/2$ and $+1/2$ are predominantly in the $\omega = -1/2$ state near $\theta = 180°$, which corresponds to the *upper* adiabat rather than the lower one. The $P = -3/2$ and $-1/2$ wavefunctions show similar behavior around $\theta = 0$. This is not the behavior implied by Eq. 15.

IV. ELECTRONIC SPECTRUM CALCULATION

A. Transition wavenumbers

In order to calculate the line positions in the vibrationally resolved $A\ ^2\Sigma^+ \leftarrow X\ ^2\Pi$ electronic spectrum, we require the bound-state energies for the excited electronic state, as well as those for the ground state. For the $A\ ^2\Sigma^+$ state we make use of the recent PES presented by Hirst *et al.*[22] This surface has a global minimum of -742.5 cm^{-1} at the linear Ar–H-S conformation ($\theta = 0°$), and a secondary minimum of -673.7 cm^{-1} for linear Ar–S-H ($\theta = 180°$). The two minima are separated by a barrier more than 600 cm^{-1} high and the lowest-energy vibrational levels are localised within one or other of the two wells.

The bound states of this PES have been analysed previously[22] and only a brief discussion is given here. Bound-state energies were calculated as eigenvalues of the spin-free triatomic Hamiltonian in Jacobi coordinates. Discrete variable representations (DVRs) were employed for both the intermolecular distance R and the angle θ. For R, 120 sinc-DVR functions[48] were used, with DVR points ranging from 2.5 Å to 8.5 Å. For θ, a 64-point DVR based on Legendre polynomials was used. With this basis set, the bound levels of interest were converged to at least seven significant figures. The resulting levels are labeled by quantum numbers $(v_{\rm SH}, b^K, n)$, where $v_{\rm SH}$ and n are quantum numbers for the SH stretch and the atom–diatom stretch respectively. K is the projection of the total angular momentum of the diatom, neglecting spin, onto the body-fixed z-axis, and b is the number of nodes in the intermolecular angle θ. The resulting energies for levels with total angular momentum $N = 0$ (neglecting spin) are in precise agreement with previous results.[22] To

facilitate the calculation of band intensities, for $N = 1$ the helicity decoupled approximation was employed, in which the Coriolis terms coupling different K-levels are ignored. The helicity-decoupled energies are within 0.5 cm^{-1} of the full close-coupled results.[22]

For the purpose of calculating transition frequencies, the asymptotic separation of the potentials is taken to be the experimental excitation energy from the $v = 0,\ j = 3/2$ level of the $^2\Pi_{3/2}$ state to the lowest $v = 0,\ j = 1/2$ level of the $^2\Sigma^+$ state of isolated SH, which is 30832.68 cm^{-1}.[49] All transitions of the complex were assumed to originate from the $P = +3/2$ level of Ar–SH ($^2\Pi$). The lowest-energy transition frequency for the complex is calculated to be 30488.5 cm^{-1}, which is 31.5 cm^{-1} greater than the experimental value of 30457 cm^{-1}.[20] This agreement is reasonable, considering the level of theory used in the calculation of the potentials.

B. Transition dipole moments

Calculations of spectroscopic intensities require transition dipole moments $\mu_{\rm tot}^{\rm if}$, where

$$\mu_{\rm tot}^{\rm if} = \langle {\rm i}|\mu_{\rm el}|{\rm f}\rangle\,. \tag{19}$$

The integrals involve the initial (i) and final (f) wavefunctions as determined from bound-state calculations. In this work we evaluated transition dipoles over *internal* coordinates (R, θ), neglecting overall rotation. This gives transition dipoles that correspond to band intensities between intermolecular vibrational states. The electronic dipole moment, $\mu_{\rm el}$, is in general a parametric function of the nuclear coordinates. In the body-fixed frame it may be expanded in terms of reduced rotation matrices,

$$\mu_{\rm el}(R,\theta) = \sum_j \mu_{{\rm el},j}^{\Delta\lambda}(R) d^j_{\Delta P,\Delta\lambda}(\theta), \tag{20}$$

where $\Delta P = P_{\rm i} - P_{\rm f}$ and $\Delta\lambda = \lambda_{\rm i} - \lambda_{\rm f}$. In the excited electronic state, $P = K \pm \frac{1}{2}$. In this work it is assumed that $\mu_{\rm el}$ consists purely of contributions from the SH monomer, so that only $j = 1$ contributes in Eq. 20 and the coefficients $\mu_{{\rm el},j}^{\Delta\lambda}$ are independent of R. Since we are dealing with a perpendicular transition in SH, $\Delta\lambda = \pm 1$. The transition dipoles were calculated as one-dimensional Gaussian quadratures in θ, then integrated over R.

C. Intensities and lifetime factors

The signals in a pulsed-laser fluorescence excitation experiment decay exponentially following each pulse, with a lifetime equal to that of the excited state being probed. Intensities are typically measured as the area under the decay curve, and so the experimental intensities are proportional to the lifetime of the excited state. Ar–SH is somewhat unusual in the large range of lifetimes exhibited by different vibrational levels in the A state. It is known that the presence of the Ar atom blocks the electronic predissociation of the SH radical, leading to a greatly increased lifetime of up to 600 ns for low-lying bound levels, compared to ~ 1 ns for the uncomplexed species.[20,50] However, the actual lifetime depends on the degree of vibrational excitation, and lifetimes specific to particular levels have been calculated by McCoy.[50]

The top panel of Fig. 7 shows a spectrum calculated directly from the squares of transition dipoles, while the center panel shows a spectrum in which the intensities have been multiplied by McCoy's lifetime values. Clearly this is possible only for levels for which lifetime data exist, and transitions to other levels are omitted in the center panel (*i.e.*, it is assumed that their lifetimes are small). Also shown is an experimental spectrum from Ref. 20. The spacings between the peaks in the calculated Ar–SH spectrum are consistently $\sim 5\%$ smaller than in experiment. It is clear that the intensity distributions are significantly different in the two calculated spectra, and that the one that includes lifetime factors gives considerably better agreement with experiment. The agreement in intensities is quite good, especially considering that the experimental spectrum was most likely not normalised for dye laser power.[51] From our results it seems likely that the small peak at ~ 30810 cm^{-1} in the experimental spectrum can be assigned to the transition to $(0, 0^0, 6)$.

Even without the lifetime weighting, transitions to levels localized in the $\theta = 180^\circ$ well of the A state, which are labelled with + symbols in Fig. 7, are weak in the simulated spectrum. This arises because of poor overlap with the $P = +3/2$ ground-state wavefunction (which is concentrated around $\theta = 0$). In addition, it is likely that such levels have short lifetimes close to that of uncomplexed SH[22] and so will have even lower intensities in the fluorescence excitation spectrum. These levels have not been observed experimentally to our knowledge.

V. SUMMARY

We have obtained new *ab initio* potential energy surfaces for the Ar–SH complex in its ground $^2\Pi$ electronic state and used them to calculate bound-state energies and wavefunctions using coupled-channel methods. We have also described a new adiabatic approximation that includes spin-orbit coupling and can be used to calculate bound states on a single potential energy surface. However, the adiabatic wavefunctions fail to reproduce some features of the true wavefunctions. We have used our results to simulate the vibrationally resolved laser-induced fluorescence excitation spectrum of Ar–SH, with intensities modelled using calculated transition dipole moments and calculated lifetimes. The inclusion of the lifetime factor is important to obtain satisfactory agreement with the experimental intensities.

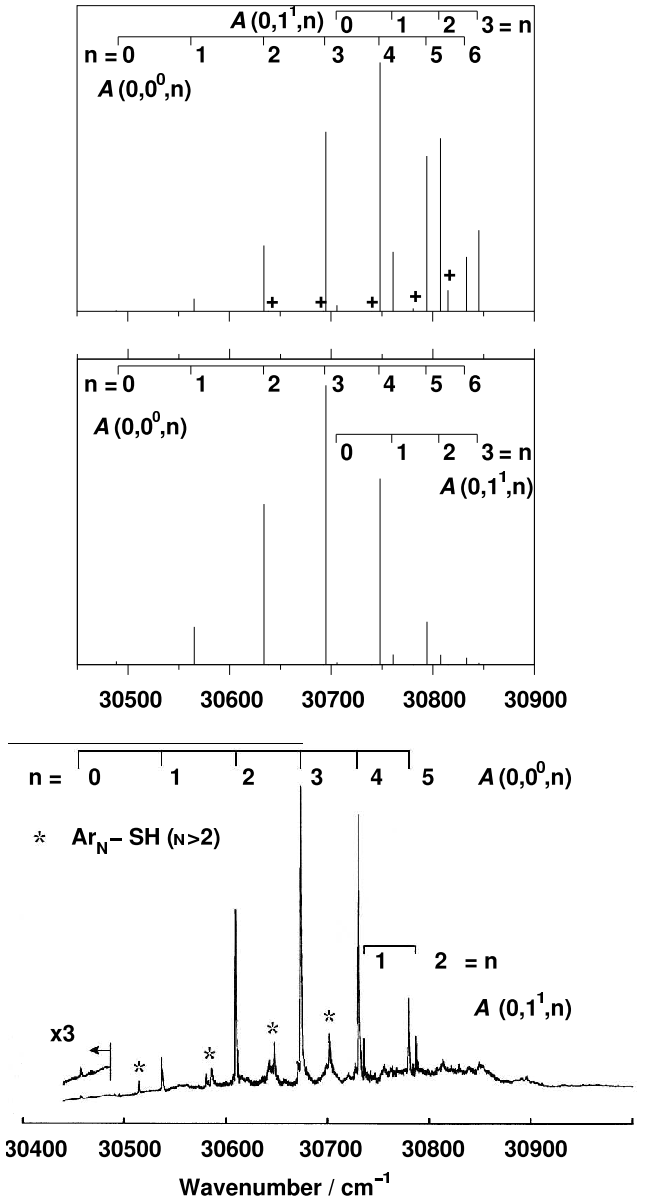


FIG. 7: Calculated vibrationally resolved fluorescence-excitation spectrum of Ar–SH for the $A\ ^2\Sigma^+ - X\ ^2\Pi$ electronic transition. The lifetime weighting of the intensities is absent for the the top panel, and present for the middle panel. Lines labeled with + indicate transitions to the $\theta = 180^\circ$ well of the A state. For comparison, the experimental spectrum is shown in the bottom panel, taken from Ref. 20. Note that the experimental spectrum contains contributions from Ar_2–SH and larger clusters as well as Ar–SH.

VI. ACKNOWLEDGEMENTS

The authors would like to thank Terry Miller for providing his experimental spectrum. RJD also thanks Dr. Stuart Mackenzie for helpful discussions, and is grateful to the Engineering and Physical Sciences Research Council (EPSRC) for funding.

[1] M. L. Dubernet, D. Flower, and J. M. Hutson, J. Chem. Phys. **94**, 7602 (1991).
[2] M. L. Dubernet and J. M. Hutson, J. Chem. Phys. **101**, 1939 (1994).
[3] M. H. Alexander, G. Capecchi, and H. J. Werner, Faraday Discuss. **127**, 59 (2004).
[4] B. Retail, J. K. Pearce, C. Murray, and A. J. Orr-Ewing, J. Chem. Phys. **122**, 101101 (2005).
[5] M. Ziemkiewicz, M. Wojcik, and D. J. Nesbitt, J. Chem. Phys. **123**, 224307 (2005).
[6] R. A. Loomis and M. I. Lester, Annu. Rev. Phys. Chem. **48**, 643 (1997).

[7] K. Liu, A. Kolessov, J. W. Partin, I. Bezel, and C. Wittig, Chem. Phys. Lett. **299**, 374 (1999).

[8] M. D. Wheeler, D. T. Anderson, and M. I. Lester, Int. Rev. Phys. Chem. **19**, 501 (2000).

[9] M. I. Lester, B. V. Pond, M. D. Marshall, D. T. Anderson, L. B. Harding, and A. F. Wagner, Faraday Discuss. **118**, 373 (2001).

[10] J. M. Merritt, J. Kupper, and R. E. Miller, Phys. Chem. Chem. Phys. **7**, 67 (2005).

[11] M. L. Dubernet and J. M. Hutson, J. Phys. Chem. **98**, 5844 (1994).

[12] M. Meuwly and J. M. Hutson, J. Chem. Phys. **119**, 8873 (2003).

[13] J. Kłos, M. M. Szczesniak, and G. Chałasinski, Int. Rev. Phys. Chem. **23**, 541 (2004).

[14] A. V. Fishchuk, P. E. S. Wormer, and A. van der Avoird, J. Phys. Chem. A **110**, 5273 (2006).

[15] D. Skouteris, D. E. Manolopoulos, W. S. Bian, H. J. Werner, L. H. Lai, and K. P. Liu, Science **286**, 1713 (1999).

[16] T. Xie, D. Wang, and J. M. Bowman, J. Chem. Phys. **116**, 7461 (2002).

[17] D. M. Neumark, Phys. Chem. Comm. **5**, 76 (2002).

[18] D. M. Neumark, Phys. Chem. Chem. Phys. **7**, 433 (2005).

[19] M.-C. Yang, A. P. Salzberg, B.-C. Chang, C. C. Carter, and T. A. Miller, J. Chem. Phys. **98**, 4301 (1993).

[20] P. Korambath, X. T. Wu, E. F. Hayes, C. C. Carter, and T. A. Miller, J. Chem. Phys. **107**, 3460 (1997).

[21] M.-C. Yang, C. C. Carter, and T. A. Miller, J. Chem. Phys. **110**, 7305 (1999).

[22] D. M. Hirst, R. J. Doyle, and S. R. Mackenzie, Phys. Chem. Chem. Phys. **6**, 5463 (2004).

[23] Y. Sumiyoshi, Y. Endo, and Y. Ohshima, J. Chem. Phys. **113**, 10121 (2000).

[24] Y. Sumiyoshi, Y. Endo, and Y. Ohshima, J. Molec. Spectrosc. **222**, 22 (2003).

[25] Y. Sumiyoshi, H. Katsunuma, K. Suma, and Y. Endo, J. Chem. Phys. **123**, 054324 (2005).

[26] Y. Sumiyoshi and Y. Endo, J. Chem. Phys. **123**, 054325 (2005).

[27] C. C. Carter, H.-S. Lee, A. B. McCoy, and T. A. Miller, J. Molec. Spectrosc. **525**, 1 (2000).

[28] M. C. Heaven, Int. Rev. Phys. Chem. **24**, 375 (2005).

[29] K. Huber and G. Herzberg, *Molecular Spectra and Molecular Structure IV. Constants of Diatomic Molecules* (Van Nostrand Reinhold, New York, 1979).

[30] H.-J. Werner, P. J. Knowles, R. Lindh, M. Schütz, P. Celani, T. Korona, F. R. Manby, G. Rauhut, R. D. Amos, A. Bernhardsson, et al., *Molpro, version 2002.6, a package of ab initio programs* (2003), see http://www.molpro.net.

[31] P. J. Knowles, C. Hampel, and H.-J. Werner, J. Chem. Phys. **99**, 5219 (1993).

[32] P. J. Knowles, C. Hampel, and H.-J. Werner, J. Chem. Phys. **112**, 3106 (1993).

[33] T. H. Dunning Jr., J. Chem. Phys. **90**, 1007 (1989).

[34] R. A. Kendall, T. H. Dunning Jr., and R. J. Harrison, J. Chem. Phys. **96**, 6796 (1992).

[35] D. E. Woon and T. H. Dunning Jr., J. Chem. Phys. **100**, 2975 (1994).

[36] S. F. Boys and F. Bernardi, Mol. Phys. **19**, 553 (1970).

[37] S. M. Cybulski, R. R. Toczylowski, H. S. Lee, and A. B. McCoy, J. Chem. Phys. **113**, 9549 (2000).

[38] K. Suma, Y. Sumiyoshi, and Y. Endo, J. Chem. Phys. **120**, 6935 (2004).

[39] D. M. Brink and G. R. Satchler, *Angular Momentum* (Clarendon Press, Oxford, 1994), 3rd ed.

[40] J. M. Brown and A. Carrington, *Rotational Spectroscopy of Diatomic Molecules* (Cambridge University Press, Cambridge, 2003).

[41] J. M. Hutson, BOUND computer code, version 15 (2006).

[42] B. R. Johnson, J. Chem. Phys. **69**, 4678 (1978).

[43] J. M. Hutson, Comput. Phys. Commun. **84**, 1 (1994).

[44] M. L. Dubernet and J. M. Hutson, J. Chem. Phys. **99**, 7477 (1993).

[45] M. L. Dubernet, P. A. Tuckey, and J. M. Hutson, Chem. Phys. Lett. **193**, 355 (1992).

[46] M. Meuwly and J. M. Hutson, J. Chem. Phys. **110**, 3418 (1999).

[47] A. E. Thornley and J. M. Hutson, J. Chem. Phys. **101**, 5578 (1994).

[48] D. T. Colbert and W. H. Miller, J. Chem. Phys. **96**, 1982 (1992).

[49] D. A. Ramsay, J. Chem. Phys. **20**, 1920 (1952).

[50] A. B. McCoy, J. Chem. Phys. **109**, 170 (1998).

[51] T. A. Miller, private communication (2006).

[52] We adopt the convention of using *lower-case* letters for all quantities that refer to *monomers*, and reserve upper-case letters for quantities that refer to the complex as a whole.